C. R. Geoscience 345 (2013) 167–175

Contents lists available at SciVerse ScienceDirect

Comptes Rendus Geoscience

www.sciencedirect.com

External geophysics, climate

On the recent global mean sea level changes: Trend extraction and El Niño's impact

Sur les variations récentes du niveau moyen global des océans : tendance et impact d'El Niño

Mahdi Haddad *, Habib Taibi, Si Mohammed Mohammed Arezki

Centre of Space Techniques, Division of Space Geodesy, 1, avenue de Palestine, BP 13, Arzew, Oran, Algeria

ARTICLE INFO

Article history:
Received 20 September 2012
Accepted after revision 5 March 2013
Available online 6 June 2013

Keywords:
Global mean sea level (GMSL)
Sea level anomaly (SLA)
Sea surface temperature anomaly (SSTA)
Cross wavelet transform (XWT)
Wavelet coherence (WTC)

Abbreviations:
AIC, Akaike information criterium
AVISO, *Archivage, validation et interprétation des données des satellites océanographiques*
CWT, Continuous wavelet transform
ENSO, El Niño-southern oscillation
ERSST, Extended reconstruction sea surface temperatures
NCDC, National Climatic Data Center
GDR, Geophysical data records
GMSL, Global mean sea level
IRW, Integrated random walk
MGDR, Merged geophysical data record
NVR, Noise variance ratio
SLA, Sea level anomaly
SSTA, Sea surface temperature anomaly
TOPEX, Ocean topography experiment
TVP, Time variable parameters
UCM, Unobserved components model
WTC, Wavelet coherence
XWT, Cross wavelet transform

ABSTRACT

The spatial sampling offered by TOPEX and Jason series of satellite radar altimeters and its continuity during the last twenty years are major assets to provide an improved vision of the global mean sea level (GMSL). The objective of this paper is to examine the recent GMSL variations (1993–2012) and to investigate the correlation between the GMSL and ENSO (El Niño-southern oscillation) episodes. For this purpose, a mean sea level anomalies time series, obtained from TOPEX, Jason-1 and Jason-2 measurements, is used to determine the trend of GMSL changes by using a simplified form of an unobserved components model (namely UCM). Then, to investigate the impact of the ENSO phenomenon on the GMSL changes, we considered the sea surface temperature anomalies (SSTA) index over the Niño3 region (5N–5S 150W–90W). Cross wavelet transform and wavelet coherence analysis are performed to expose common power between the GMSL changes and the SSTA index and their relative phase in the time–frequency space. The results indicate that there are in the estimated GMSL's trend a number of fluctuations over short periods that are least partly related to the El Niño/La Niña episodes. Cross wavelet transform and wavelet coherence analysis indicate that a significant correlation between GMSL and ENSO occurred during 1997–1998, 2006–2007, 2009–2010 El Niño events and 2007–2008 and 2010–2011 La Niña ones. All these areas show in-phase relationship, suggesting that GMSL and SSTA index vary synchronously.

* Corresponding author.
E-mail address: haddad_mahdi@yahoo.fr (M. Haddad).

1631-0713/$ – see front matter
http://dx.doi.org/10.1016/j.crte.2013.03.002

1. Introduction

Global mean sea level (GMSL) change is a considerable interest variable in climate change studies. The measurement of changes in sea level can provide an important corroboration of predictions by climate models of global warming. For the past century, tide gauges show that global mean sea level rose at a rate of around 1.7 mm/year (Church and White, 2011). More recently and during the satellite era of sea level measurement (1993–2009), the rate of rise is estimated at around 3.2 ± 0.4 mm/year from the satellite data (Cazenave and Llovel, 2010; Church and White, 2011; Mitchum et al., 2010; Nerem et al., 2010) and 2.8 ± 0.8 mm/year from in-situ data (Church and White, 2011). This rate is significantly higher than the mean rate recorded by tide gauges over the past century.

The main factors causing current global mean sea level rise are thermal expansion of seawaters, land ice loss and water mass exchange between oceans and land water reservoirs. On average, over the satellite altimetry era (1993–2010), the contribution of ocean warming to the observed sea level rise is about 30% (Cazenave and Llovel, 2010; Cazenave and Remy, 2011; Church et al., 2011), while the contribution of glaciers and ice caps is accounted for $\sim$30% of sea level rise (Church et al., 2011; Cogley, 2009; Steffen et al., 2010). Although not constant through time, on average over 1993–2010, ice sheets mass loss explains $\sim$20% of the rate of sea level rise (Cazenave and Remy, 2011; Church et al., 2011; Steffen et al., 2010). A review of sea level evolution, globally and regionally, during the 20th century and the last two decades and the contributions to recent GMSL rise is given in Meyssignac and Cazenave (2012).

Recent studies have been aimed at explaining the influence of ENSO on the global mean sea level, which might result from changes in either global ocean heat content or global ocean mass. Considering the Multivariate ENSO Index (MEI) over 1993–2010, Nerem et al. (2010) noticed that detrended GMSL changes are correlated with ENSO occurrences, with positive/negative sea level anomalies observed during El Niño/La Niña events. Strong El Niño events have the potential to temporarily increase the global sea level (Cazenave et al., 2012; Ngo-Duc et al., 2005), whereas in the cold La Niña phase, the opposite occurs and sea level may exhibit a temporary fall.

Based on a global water mass conservation approach using GRACE satellite data and the (ISBA–TRIP) global hydrological model developed by Météo France (Alkama et al., 2010), Llovel et al. (2011) showed the close relationship between the interannual global mean sea level changes and land water storage variations, with a tendency for a deficit in land water storage during El Niño events, and vice versa during La Niña (with the Amazon basin as a dominant contributor to the latter).

Recent investigations suggest in addition that positive/negative mean sea level anomalies during El Niño/La Niña essentially result from positive/negative mass anomalies in the north tropical Pacific Ocean, possibly associated with reduced/increased transport of Pacific waters into the Indian Ocean through the Indonesian straits (Cazenave et al., 2012). Using a combination of GRACE satellite data and in-situ ocean temperature and rainfall data, Boening et al. (2012) show that during the 2011 strong La Niña event, the change in the sea level is due to water mass temporarily shifting from oceans to land as precipitation increased over Australia, northern South America, and Southeast Asia, while it decreased over the oceans. This study presents the first direct observation of the ENSO-induced exchange of freshwater that drives interannual changes in GMSL.

In this paper and at the first stage, we aim to provide a description of the global mean sea level variations. For this purpose, an unobserved components model (Young et al., 1999) based on a trend plus an auto-regression (AR) component is used to investigate homogeneous measurements of mean sea level anomalies datasets from the TOPEX and Jason series of satellite radar altimeters. The GMSL trend is extracted from the time series and a perturbational component about the trend is modelled as a pure AR component. Such an approach is useful in cases where the periodic behaviour of the perturbation about the trend is not very marked.

In the second stage, we investigate the impact of the ENSO phenomenon on the GMSL changes. For this, we considered the sea surface temperature anomalies (SSTA) index over the Niño3 region (5°N to 5°S, 150°W to 90°W). The cross wavelet transform and wavelet coherence analysis (Grinsted et al., 2004) are used for examining relationships in time-frequency space between the two time series of GMSL and SSTA.

The rest of the paper is organized as follows. Section 2 describes the two datasets used in this study. The two models used for trend extraction and for the coherence analysis are briefly explained in Section 3. Section 4 describes the application of UCM for GMSL time series analysis. The UCM model is used to interpolate the datasets over periods when measurements are missing and to decompose the time series into trend and harmonic components. Furthermore, this section uses the cross wavelet transform and wavelet coherence analysis to localize similarities in time and scale between the global mean sea level and Niño3 SSTA time series. The empirical results are addressed in this section. Section 5 concludes.

2. The data

2.1. Global mean sea level reference series

Radar altimeters permanently transmit signals to the Earth, and receive the reflected echo from the sea surface. The satellite orbit has to be accurately tracked and its position is determined relative to a reference surface (an ellipsoid). The sea surface height (SSH) is calculated by subtracting the measured distance between the satellite and sea surface from the precise orbit of the satellite. The sea level anomalies (SLA), defined as variations of the sea surface height (SSH) with respect to an a priori mean sea surface (MSS), are generally used as precious and main indicators for the development of scientific applications that aim to study the ocean variability (mesoscale circulation, seasonal variations, El Niño...).

Table 1
Altimetry data processing parameters and corrections.

Parameters	TOPEX	Jason-1	Jason-2
Time period	Dec. 06, 1992 to Jan. 10, 2002	Jan. 15, 2002 to July 2, 2008	July 3, 2008 to present
Cycles	8–343	1–239	1–current
Base data set	MGDR-B	GDR-C	GDR-T
Orbit	STD0905 (Lemoine et al., 2010)		
Range & corrections			
Waveform tracker	GDR		
Dry troposphere	GDR (from ECMWF)		
Wet troposphere	TMR (Replacement Product v.1.0)	GDR-C (Cycles 1–227); JMR Replacement Product (Cycles 228–259)	AMR (GDR)
Ionosphere	GDR		
Sea state bias	CLS Collinear v. 2009 (Tran et al., 2010)		
Center of gravity	MGDR-B	N/A	
Mean sea surface & corrections			
Mean sea surface	CLS01 (Hernandez and Schaeffer, 2001)		
Ocean tide & loading tide	GOT4.7 (Ray, 1999)		
Solid earth tide	GDR (Cartwright and Tayler, 1971; Cartwright and Edden, 1973)		
Pole tide	GDR (Wahr, 1985)		
Atmospheric pressure (inverted barometer)	AVISO dynamic atmosphere correction (DAC) that combines MOG2D high-frequency and inverted barometer low-frequency signals (Pascual et al., 2008)		
Glacial isostatic adjustment (GIA)	−0.3 mm/year (Peltier, 2001, 2002, 2009; Peltier and Luthcke, 2009)		
Processing corrections			
Inter-mission bias	88.48 mm (TOPEX to Jason-1)	58.52 mm (Jason-1 to Jason-2)	
Minimum ocean depth	120 m		
Outlier removal	Anomaly greater than 2 m		

GDR: geophysical data records; MGDR: merged geophysical data record; AVISO: *archivage, validation et interprétation des données des satellites océanographiques*; TOPEX: ocean topography experiment.

In our research, we investigate a temporal series of averaged sea level anomalies (SLA) over all oceans and seas for the entire altimetry period, obtained by combining the time series from all three TOPEX, Jason-1 and Jason-2 missions (Nerem et al., 2010). These datasets were provided by the CU Sea Level Research Group of the University of Colorado[1]. This series covers the time period from the beginning of 1993 to the end of 2012 (20 years), with a sampling rate of 10 days.

The used mean sea level anomalies series is represented on Fig. 1. The main input data for computing this series are the Geophysical Data Records produced by NASA and CNES (TOPEX, Jason-1, Jason-2), which are therefore of the highest quality, notably in orbit determination. The three missions are linked together during the "verification" phases of the Jason-1 and Jason-2 missions in order to calculate very precisely the bias in GMSL between these missions. TOPEX and Jason-1 were connected by applying a bias of 88.48 mm to Jason-1's GMSL. Similarly, Jason-2's GMSL was connected to Jason-1's GMSL by applying a bias of 58.52 mm to Jason-2's GMSL and also by adding the bias between Jason-1 and TOPEX/Poseidon. All of the standard corrections to the altimeter range were applied to the sea surface height (SSH), including removal of ocean tides and an inverted barometer correction. The used mean sea surface (MSS) is the CLS01 model (Hernandez and Schaeffer, 2001), obtained from 7 years of TOPEX/Poseidon data, 5 years of ERS-1/2 data, 2 years of Geosat data added to ERS-1 geodetic data, which were processed and homogenized in order to produce a $(1/30^\circ \times 1/30^\circ)$ gridded map. Table 1 describes the parameters used by the University of Colorado for computing global mean sea level reference series.

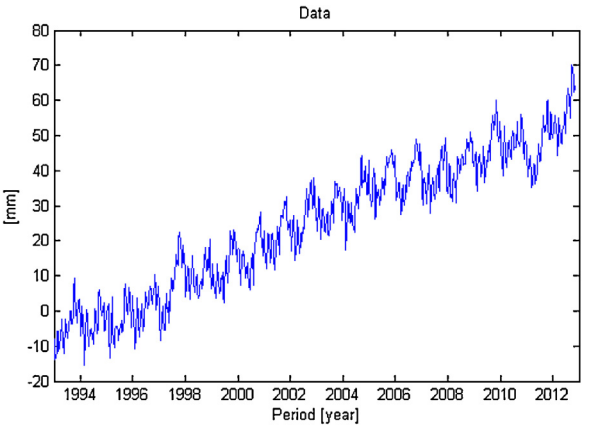

Fig. 1. Global mean sea level anomalies time series (1993–2012).

[1] http://sealevel.colorado.edu/.

2.2. Sea surface temperature anomalies series

Monitoring of ENSO conditions primarily focuses on the sea surface temperature anomaly (SSTA) index (variations from an average or other statistical reference value) in the equatorial Pacific. SSTA equal to or greater than 0.5 °C in the Niño3 region (5°N to 5°S, 150°W to 90°W), or exceeding 0.4 °C in the Niño3.4 region (5°N to 5°S, 170°W to 120°W), could indicate ENSO warm phase (El Niño) conditions (Trenberth, 1997), while anomalies less than or equal to −0.5 °C (or −0.4 °C for the Niño3.4 region) are associated with cool phase (La Niña) conditions.

In this paper, the used ENSO index was the average of SSTA computed over the Niño3 region (5°S to 5°N, 90°W to 150°W), with respect to a 1971–2000 month climatology (Xue et al., 2003). These data sets were obtained from the most recent version (v3b) of the NCDC Extended Reconstruction Sea Surface Temperatures (ERSST) analysis[2], monthly from January 1880 to June 2010. ERSST.v3b was generated using in-situ Sea Surface Temperature (SST) data and improved statistical methods that allow stable reconstruction using sparse data. The monthly analysis extends from January 1854 to the present, but because of sparse data in the early years, the analyzed signal was damped before 1880. After 1880, the strength of the signal was more consistent over time. ERSST is suitable for long-term global and basin wide studies; local and short-term variations have been smoothed in ERSST. The ERSST.v3b analysis is exactly as described in the ERSST.v3 paper (Smith et al., 2008), with one exception: satellite SST data are not used in ERSST.v3b.

3. Methodology

3.1. The unobserved components model (UCM)

The UCM are models in which time series are decomposed as the sum or a product of a number of other simple time series with economic or physical meaning. One widely accepted univariate version of UCM is (Young et al., 1999):

$$y_t = T_t + C_t + S_t + f(u_t) + N_t + e_t, \qquad e_t \sim N(0, \sigma^2) \qquad (1)$$

where y_t is the observed time series; T_t is a trend or low-frequency component; C_t is a sustained cyclical or quasi-cyclical component (e.g., an economic cycle) with period different from that of any seasonality in the data; S_t is a seasonal component (e.g., annual seasonality); $f(u_t)$ captures the influence of a vector of exogenous variables u_t, if necessary including stochastic, nonlinear static or dynamic relationships; N_t is an stochastic perturbation model (i.e. colored noise modeled as an auto-regression, namely auto-regression (AR) or autoregressive moving average, namely ARMA process), and e_t is an 'irregular' component, normally defined for analytical convenience as a normally distributed Gaussian sequence with zero mean value and variance σ^2. In order to allow for non-steadiness in the time series y_t, the various components in the model, including the trend T_t, can be characterized by stochastic, time variable parameters (TVP's), with each TVP defined as a non-stationary stochastic variable, as discussed below.

In practice, not all the components in eq. (1) are necessary: indeed, the simultaneous presence of all these components can induce identification problems and so use of the complete model (1) is not advisable in practice unless adequate precautions are taken. In this paper, the simplified used model is one such decomposition that contains only the trend plus an AR component, seasonal and white noise components.

The trend component is formulated in a stochastic state space context and then solved by using an integrated random walk (IRW) plus noise modelling approach. The full state space description is given by the state equation (Pedregal and Trapero, 2007):

$$\begin{bmatrix} x_{1t} \\ x_{2t} \end{bmatrix} = \begin{bmatrix} 1 & 1 \\ 0 & 1 \end{bmatrix} \begin{bmatrix} x_{1t-1} \\ x_{2t-1} \end{bmatrix} + \begin{bmatrix} 0 \\ 1 \end{bmatrix} \eta_{t-1} \qquad (2)$$

and the observation equation of the trend component,

$$T_t = \begin{pmatrix} 1 & 0 \end{pmatrix} \begin{pmatrix} x_{1t} \\ x_{2t} \end{pmatrix} \qquad (3)$$

x_{1t} is the first state variable known as the 'level', x_{2t} is the second state variable and generally known as the 'slope', η_t is a zero mean, serially uncorrelated white noise process with a certain variance. Young et al. (1999, 2007) also defined two parameters for computing convenience: noise variance ratio (NVR) Q_r and $\hat{p}_t$. Q_r is a normalized matrix of the diagonal noise variance matrix Q, and $\hat{p}_t$ is the error covariance matrix associated with the estimation state. Young et al. (1999) propose one final simplification using the estimate of the trend from an autoregressive (AR) model. The AR order is identified by the Akaike's Information Criterion (AIC), whereas, the seasonal term is modelled as a sum of the fundamental signal and of its associated harmonics:

$$S_t = \sum_{i=1}^{N} \left[a_{i,t} \cos(\omega_i t) \; + \; b_{i,t} \sin(\omega_i t) \right] \qquad (4)$$

where $a_{i,t}$ and $b_{i,t}$ are stochastic TVP's and ω_i are the frequencies related to the time series, revealed by an autoregressive spectrum (Tych et al., 2002).

3.2. Cross wavelet transform and wavelet coherence

The cross wavelet transform and wavelet coherence analysis used in this paper follows the method of Grinsted et al. (2004). Although the basic components of this analysis are reviewed here, readers are referred to Grinsted et al. (2004) for a more detailed explanation.

The continuous wavelet transform (CWT) allows analyzing the temporal evolution of the frequency content of a given signal or timing series. The *CWT* of a time series (x_n, $n = 1, \ldots, N$), with uniform time steps δt, is defined as the convolution of x_n with the scaled and normalized

[2] http://www.ncdc.noaa.gov/ersst/.

wavelet:

$$W_n^x(s) = \sqrt{\frac{\delta t}{s}} \sum_{n'=1}^{N} x_{n'} \psi_0 \left[(n' - n) \frac{\delta t}{s} \right] \quad (5)$$

where ψ_0 is the dimensionless frequency, and the parameter s is the "dilation" parameter used to change the scale.

The wavelet power is defined as $\left|W_n^x(s)\right|^2$. The complex argument of $W_n^x(s)$ can be interpreted as the local phase (Torrence and Compo, 1998).

From two CWTs we construct the cross wavelet transform (*XWT*), which will expose their common power and relative phase in time–frequency space. The *XWT* of two time series x_n and y_n is defined as:

$$W^{XY} = W^X W^{Y^*} \quad (6)$$

where * denotes complex conjugation. Furthermore, the cross wavelet power is defined as $\left|W^{XY}\right|$. The complex argument of W^{XY} can be interpreted as the local relative phase between *xn* and y_n in the time–frequency space.

Following Torrence and Webster (1999), the wavelet coherence (WTC) of two time series, which can find significant coherence even though the common power is low, is defined as:

$$R_n^2(s) = \frac{\left|S\left(s^{-1} W_n^{XY}(s)\right)\right|^2}{S\left(s^{-1}\left|W_n^X(s)\right|^2\right) \cdot S\left(s^{-1}\left|W_n^Y(s)\right|^2\right)} \quad (7)$$

S is a smoothing operator: $S(W) = S_{scale}(S_{time}(W_n(s)))$, where S_{scale} denotes smoothing along the wavelet scale axis and S_{time} smoothing in time.

4. Results and discussion

4.1. Global mean sea level reference series analysis

All of the results in this section are obtained by means of the Captain Toolbox v7.5[3] (Taylor et al., 2007). The Captain Toolbox is a set of MATLAB functions for non-stationary time series analysis and forecasting. It allows the identification of unobserved components models, time variable parameter models, state-dependent parameter models and multiple-input discrete and continuous time-transfer function models. The toolbox is useful for system identification, signal extraction, interpolation, backcasting, forecasting and databased mechanistic analysis of a wide range of linear and nonlinear stochastic systems.

The global mean sea level series was decomposed into trend and seasonal components using a model based on a trend plus an AR component. Apart from the decomposition of time series into trend and seasonal components, this methodology also provides a time series model of the data, which is used for the interpolation of missing data. Note that this model can also be used for backcasting and forecasting.

In the first place, we estimated a smooth trend using an IRW with an initial noise variance ratio (NVR) hyper-parameter of 10^{-4}. The green line and the red line on Fig. 2 correspond to the smooth trend and the residuals series, respectively.

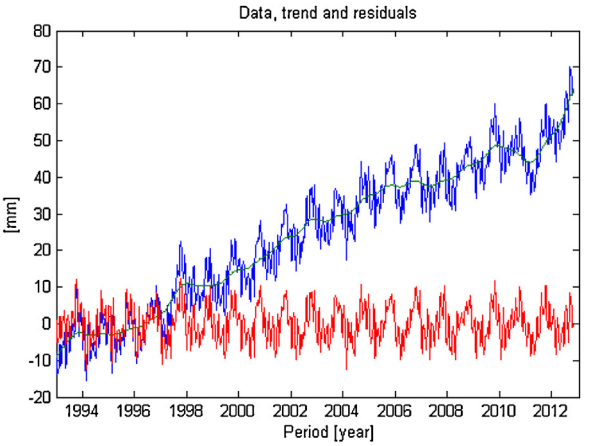

Fig. 2. Smooth trend using an integrated random walk with an initial noise variance ratio hyper-parameter of 1×10^{-4}.

Table 2
AR model for perturbations.

P	ARp	ARpse
1	−0.6999	0.0376
2	0.2256	0.0460
3	−0.0731	0.0464
4	−0.1440	0.0464
5	−0.2162	0.0459
6	−0.0995	0.0464
7	0.1631	0.0465
8	0.0605	0.0462
9	0.1918	0.0376

AR: auto-regression.

Then, the order of the autoregressive (AR) model for the perturbations is identified using the AIC. We searched for models ranging from 1st to the 10th order. The best-fit AR polynomial is obtained for an order of 9. The AR model for the perturbations is estimated, together with the associated optimal NVR for the IRW trend.

Table 2 represents the estimation results of the perturbational component about the trend, were P is the AR order for perturbations, ARp is the AR polynomials for the perturbations and ARpse is the standard error of AR parameters for perturbations.

The final trend NVR is estimated at 2.7554×10^{-4}, with a trend integration order of 2. Finally, both components (trend and seasonal component) are estimated simultaneously.

Figs. 3, 4 and 5 represent the estimated trend, the total seasonal component and the fitted data, respectively. A zoom on the final 2 years, with the standard errors, is shown on Fig. 6.

The analysis of the estimated trend indicates that the global mean sea level is subject to significant rise, from −6 mm to 62 mm during the period 1993–2012. Applying a least squares linear regression analysis to the extracted trend gives a rate of 3.22 mm/year between 1993 and 2012, with a formal error of 0.02 mm/year (see Fig. 7).

[3] http://www.es.lancs.ac.uk/cres/captain/.

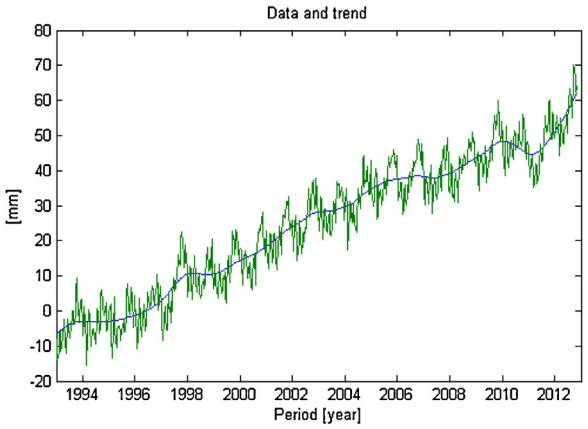

Fig. 3. Global mean sea level anomalies time series and estimated trend (1993–2012).

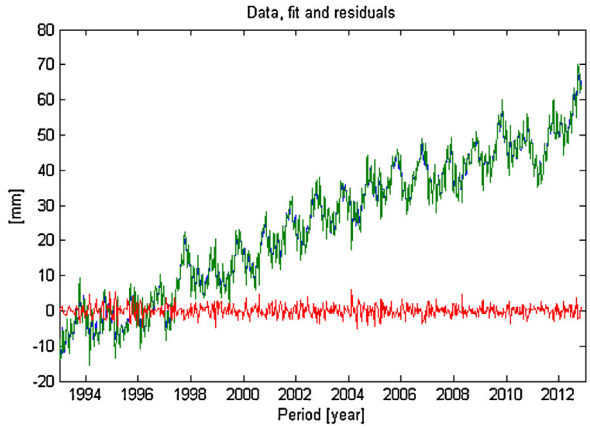

Fig. 5. Global mean sea level anomalies time series (blue line), fit model (green line) and residuals (red line).

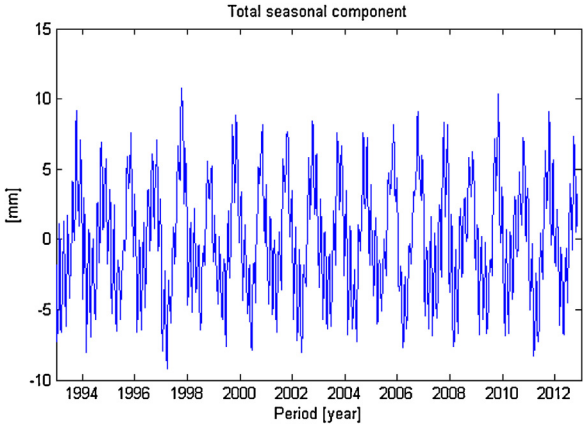

Fig. 4. Estimated total seasonal component.

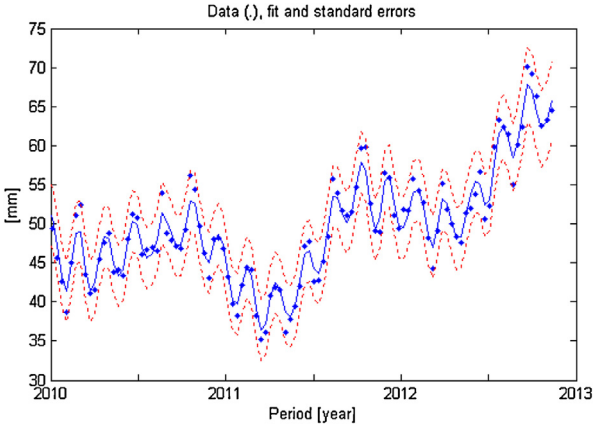

Fig. 6. Data, fit and standard errors of the final 3 years.

The estimated rate of GMSL rise agrees with the CU GMSL rate[4] over the same period of 3.2 ± 0.4 mm/year, where the realistic error assigned in this quantity (± 0.4 mm/year) is based on comparisons of altimeter heights with tide gauge-based sea level measurements (Mitchum, 2000). For further information on errors assessment affecting the calculation of the GMSL rate and comparison of altimetry-based sea level with in-situ measurements, the reader is referred to Ablain et al. (2009).

One can see on Fig. 7 evidence that there are a number of fluctuations over short periods in the estimated trend. This variability is at least partly related to El Niño/La Niña episodes (sea level rises during El Niño and falls during La Niña) and associated changes in the hydrological cycle.

4.2. Correlation between global mean sea level variability and El Niño-southern oscillation

To compare the global mean sea level to the sea surface temperature anomalies index over the Niño3 region, we removed from original global mean sea level time series (series of mean sea level anomalies) the extracted trend and the total seasonal components (both estimated in Section 4.1). Then, since ERSST.v3b SSTA data are monthly distributed, we created from the detrended GMSL datasets

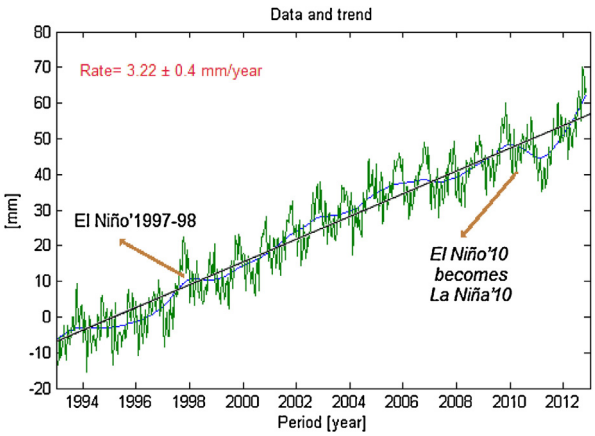

Fig. 7. Estimated trend and linear regression line.

[4] http://sealevel.colorado.edu/content/2013rel1-global-mean-sea-level-time-series-seasonal-signals-retained.

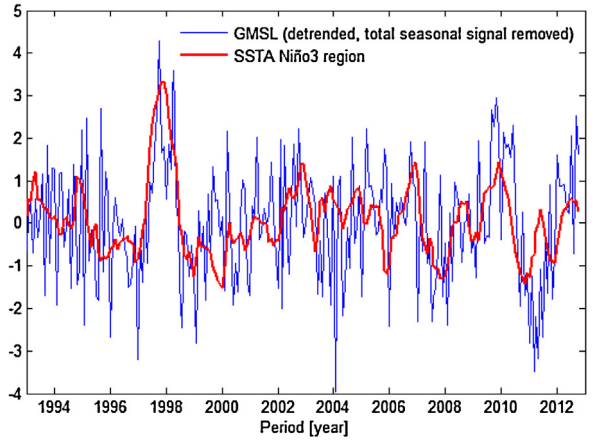

Fig. 8. Global mean sea level (detrended and total seasonal component removed) series and mean sea surface temperature anomalies series over the Niño3 region.

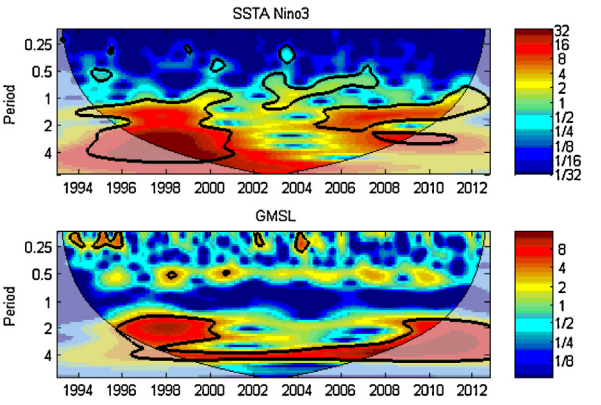

Fig. 9. Continuous wavelet power spectrum of global mean sea level time series (top) and mean sea surface temperature anomalies series over the Niño3 region (bottom). The thick black contour designates the 5% significance level against red noise, and the cone of influence where edge effects might distort the picture is shown as a lighter shade.

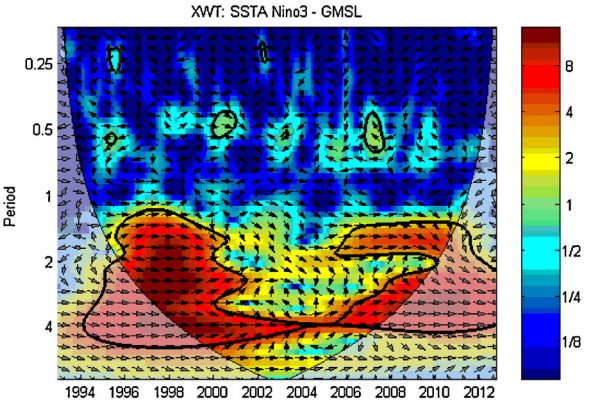

Fig. 10. Cross wavelet transform of global mean sea level and sea surface temperature anomalies series. The 5% significance level against the red noise is shown as a thick contour. The relative phase relationship is shown as arrows (with in-phase pointing right, anti-phase pointing left).

a lower resolution series with a time scale of one month to be used for relationship analysis.

Fig. 8 shows the used averaged SSTA time series (1993–2012) over the Niño3 region and the detrended and seasonally adjusted GMSL series used for correlation analysis. The plotted series show a strong correlation between the global mean sea level and the SSTA Niño3 index.

One can see from Fig. 8 evidence that there was a particularly strong warm event of large amplitude during the 1997–1998 period. The El Niño of 1997–98 was extremely severe. This event was a so-called "Type-1" El Niño (Fu et al., 1986), having the strongest averaged SSTA $> 3.0\,^{\circ}$C from October 1997 to January 1998 (see Fig. 8). Although it started in April to May 1997, its effects extended into the early summer of 1998.

In early 2006, sea surface temperature positive anomalies are measured in the central equatorial Pacific. These high-temperature anomalies characterize a new El Niño event. In early summer 2009, sea surface height positive anomalies are measured from August 2009, with a maximum during November 2009 (SSTA $> 1.1\,^{\circ}$C), characterizing a moderate El Niño event (see Fig. 8).

Severe La Niña was also formed in 1998 and 2012. From June 2007, data indicated a moderate La Niña event, which strengthened until early 2008. A new La Niña episode was developed in mid-2010, and lasted until early 2011. It intensified again in the mid-2011 (see Fig. 7). Between the beginning of 2010 and the middle of 2011, sea level fell until -3 mm. This occurred concurrently with the strong phase, La Niña 2011.

For examining strictly speaking relationships between the two time series SSTA and GMSL (detrended and total seasonal component removed) series in time–frequency space, first the CWT of both datasets was calculated. The XWT and WTC tests are then performed.

The CWT of the SSTA index and GMSL series are shown on Fig. 9. There are clearly common features in the wavelet power of the two time series in the 2–4-year band in the period from 1996 to 2000. However, the similarity between the two patterns for other periods is quite low and it is therefore hard to say whether it is significant. The cross wavelet transform helps in this regard; it will expose the common power and relative phase in the time-frequency space.

The XWT of SSTA index and GMSL and their relative phase relationship (with in-phase: arrows pointing right, anti-phase: arrows pointing left) are shown on Fig. 10. Here we note that there is a significant common power in the 1–4-year band from 1996 to 2000. Also, there is an appreciable power in the 1–2-year band from 2005–2010. All these areas show an in-phase relationship, suggesting that GMSL and SSTA vary synchronously.

The squared WTC of SSTA and GMSL is shown on Fig. 11. Compared with the XWT, a larger section stands out as being significant and all these areas show an in-phase relationship between SSTA and GMSL. Oscillations in SSTA are manifested in the GMSL on wavelengths varying from 1–4 years in the period from 1996 to 2000 (El Niño 1997–98), 1–2 years in the period from 2005 to 2008 (2006–2007 El Niño event and 2007–2008 La Niña episode). Also, there is an appreciable section in the 3–4-year band from

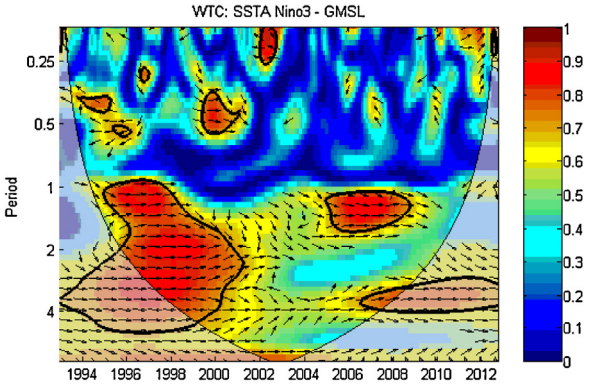

Fig. 11. Squared wavelet coherence between the sea surface temperature anomalies and global mean sea level time series. The 5% significance level against the red noise is shown as a thick contour. All significant sections show in-phase behavior.

2007–2012 (2009–2010 El Niño, 2010–2011 La Niña events), though this area is outside of the cone of influence in which edge effects are considerable.

5. Conclusions

In this paper, an approach of seasonal adjustment and trend extraction based on the unobserved components model (UCM) has been used to investigate the global mean sea level anomalies (GSLA) series. Our GMSL trend gives a rate of 3.22 ± 0.4 mm/year between 1993 and 2012. This obtained rate agrees with the study of the CU Sea Level Research Group, which suggested a sea level rise rate of 3.2 ± 0.4 mm/year over the same period. Although the extracted global trend indicates a rise in the mean level of the oceans, there are marked fluctuations over short periods.

Cross wavelet transform and wavelet coherence analysis were successfully employed to expose common power between the GMSL changes and ENSO episodes and their relative phase in time–frequency space. The results indicate a correlation between GMSL changes and ENSO episodes on wavelengths band of 1–4 years in the period from 1996 to 2000, 1–2 years in the period from 2005 to 2008 and also in the 3–4-year band from 2007–2012. This is a pertinent result of a high correlation between the GMSL variability and El Niño/La Niña episodes.

Acknowledgments

We are very grateful to the Colorado Center for Astrodynamics Research of the University of Colorado, Boulder, and the National Climatic Data Center (NCDC) for providing global mean sea level time series and ERSST.v3b SSTA data, respectively. We also thank the Centre for Research on Environmental Systems (CRES) of the Lancaster University for providing the Captain toolbox. We are enormously grateful to Anny Cazenave (LEGOS–CNES) for helpful comments and suggestions that helped us to improve our manuscript.

References

Ablain, M., Cazenave, A., Guinehut, S., Valladeau, G., 2009. A new assessment of global mean sea level from altimeters highlights a reduction of global slope from 2005 to 2008 in agreement with in-situ measurements. Ocean Sci. 5, 193–201.

Alkama, R., Decharme, B., Douville, H., Voldoire, A., Tyteca, S., Le Moigne, P., Becker, M., Cazenave, A., Sheffield, J., 2010. Global evaluation of the ISBA-TRIP continental hydrological system. Part 1: comparison to GRACE terrestrial water storage estimates and in-situ river discharges. J. Hydrometeorol. 11, 583–600, http://dx.doi.org/10.1175/2010JHM1211.

Boening, C., Willis, J.K., Landerer, F.W., Nerem, R.S., Fasullo, J., 2012. The 2011 La Niña: so strong, the oceans fell. Geophys. Res. Lett. 39, L19602, http://dx.doi.org/10.1029/2012GL053055.

Cartwright, D.E., Edden, A.C., 1973. Corrected tables of tidal harmonics. Geophys. J. Int. 33, 253–264.

Cartwright, D.E., Tayler, R.J., 1971. New computations of the tide-generating potential. Geophys. J. R. Astron. Soc. 23, 45–73.

Cazenave, A., Henry, O., Munier, S., Delcroix, T., Gordon, A.L., Meyssignac, B., Llovel, W., Palanisamy, H., Becker, M., 2012. Estimating ENSO influence on the global mean sea level, 1993–2010. Mar. Geod. 35 (Sup. 1) 82–97, http://dx.doi.org/10.1080/01490419.2012.718209.

Cazenave, A., Llovel, W., 2010. Contemporary sea level rise. Annu. Rev. Mar. Sci. 2, 145–173, http://dx.doi.org/10.1146/annurev-marine-120308-081105.

Cazenave, A., Remy, F., 2011. Sea level and climate: measurements and causes of changes, interdisciplinary reviews. Clim. Change 2 (5) 647–662, http://dx.doi.org/10.1002/wcc.139.

Church, J.A., White, N.J., 2011. Sea-level rise from the late 19th to the early 21st century. Surv. Geophys. 32 (4/5) 585–602, http://dx.doi.org/10.1007/s10712-011-9119-1.

Church, J.A., White, N.J., Konikow, L.F., Domingues, C.M., Cogley, J.G., Rignot, E., Gregory, .J.M., van den Broeke, M.R., Monaghan, A.J., Velicogna, I., 2011. Revisiting the Earth's sea level and energy budgets from 1961 to 2008. Geophys. Res. Lett. 38, L18601, http://dx.doi.org/10.1029/2011GL048794.

Cogley, J.C., 2009. Geodetic and direct mass balance measurements: comparison and joint analysis. Ann. Glaciol. 50, 96–100, http://dx.doi.org/10.3189/172756409787769744.

Fu, C., Diaz, H.F., Fletcher, J.O., 1986. Characteristics of the response of sea surface temperature in the central Pacific associated with warm episodes of the Southern Oscillation. Mon. Weather Rev. 114, 1716–1738.

Grinsted, A., Moore, J.C., Jevrejeva, S., 2004. Application of the cross wavelet transform and wavelet coherence to geophysical time series. Nonlinear Proc. Geophys. 11, 561–566.

Hernandez, F., Schaeffer, P., 2001. The CLS01 Mean Sea Surface: A Validation With the GSFC00.1 Surface. Tech. rep., CLS, Ramonville St-Agne, 14 pp.

Lemoine, F.G., Zelensky, N.P., Chinn, D.S., Pavlis, D.E., Rowlands, D.D., Beckley, B.D., Luthcke, S.B., Willis, P., Ziebart, M., Sibthorpe, A., et al., 2010. Towards development of a consistent orbit series for TOPEX, Jason-1, and Jason-2. Adv. Space Res. 46, 1513–1540.

Llovel, W., Becker, M., Cazenave, A., Jevrejeva, S., Alkama, R., Decharme, B., Douville, H., Ablain, M., Beckley, B., 2011. Terrestrial waters and sea level variations on interannual time scale. Global Planet. Change 75, 76–82, http://dx.doi.org/10.1016/j.gloplacha.2010.10.008.

Meyssignac, B., Cazenave, A., 2012. Sea level: a review of present-day and recent-past changes and variability. J. Geodyn. 58, 96–109.

Mitchum, G.T., 2000. An improved calibration of satellite altimetric heights using tide gauge sea levels with adjustment for land motion. Mar. Geod. 23, 145–166, http://dx.doi.org/10.1080/01490410050128591.

Mitchum, G.T., Nerem, R.S., Merrifield, M.A., Gehrels, W.R., 2010. Modern sea level changes estimates. In: Church, J.A., Woodworth, P.L., Aarup, T., Wilson, W.S. (Eds.), Understanding Sea Level Rise and Variability. Wiley-Blackwell Publishing, London, UK.

Nerem, R.S., Chambers, D., Choe, C., Mitchum, G.T., 2010. Estimating mean sea level change from the TOPEX and Jason Altimeter missions. Mar. Geod. 33 (sup 1) 435–446, http://dx.doi.org/10.1080/01490419.2010.491031.

Ngo-Duc, T., Laval, K., Polcher, J., Cazenave, A., 2005. Contribution of continental water to sea level variations during the 1997–1998 El Niño-Southern oscillation event: comparison between atmospheric model intercomparison project simulations and TOPEX/Poseidon satellite data. J. Geophys. Res. 110, D09103, http://dx.doi.org/10.1029/2004JD004940.

Pascual, A., Marta, M., Gomis, D., 2008. Comparing the sea level response to pressure and wind forcing of two barotropic models: Validation

with tide gauge and altimetry data. J. Geophys. Res. 113 (C07011) 16, http://dx.doi.org/10.1029/2007JC004459.
Pedregal, D.J., Trapero, J.R., 2007. Electricity prices forecasting by automatic dynamic harmonic regression models. Energy Convers. Manage. 48, 1710–1719.
Peltier, W.R., 2001. Global glacial isostatic adjustment and modern instrumental records of relative sea level history. Int. Geophys., Sea Level Rise, Hist. Consequences 75, 65–95.
Peltier, W.R., 2002. Global glacial isostatic adjustment: palaeogeodetic and space-geodetic tests of the ICE-4G (VM2) model. J. Quat. Sci. 17, 491–510.
Peltier, W.R., 2009. Closure of the budget of global sea level rise over the GRACE era: the importance and magnitudes of the required corrections for global glacial isostatic adjustment. Quat. Sci. Rev. 28, 1658–1674.
Peltier, W.R., Luthcke, S.B., 2009. On the origins of Earth rotation anomalies: new insights on the basis of both "paleogeodetic" data and gravity recovery and climate experiment (GRACE) data. J. Geophys. Res. 114, B11.
Ray, R., 1999. A Global Ocean Tide model from TOPEX/Poseidon Altimetry, GOT99. 2. NASA Tech. Memo. NASA/TM-1999-209478. Goddard Space Flight Center, NASA Greenbelt, MD, USA, 58 pp.
Smith, T.M., Reynolds, R.W., Peterson, T.C., Lawrimore, J., 2008. Improvements to NOAA's historical merged land-ocean surface temperature analysis (1880–2006). J. Climate 21, 2283–2296.
Steffen, K., Thomas, R.H., Rignot, E., Cogley, J.G., Dyurgerov1, M.B., Raper, S.C.B., Huybrechts, P., Hanna, E., 2010. Cryospheric contributions tosea level rise and variability. In: Church, J., Woodworth, P.L., Aarup, T., Wilson, W.S. (Eds.), Understanding Sea Level Rise and Variability. Wiley-Blackwell, Oxford, UK, http://dx.doi.org/10.1002/9781444323276.ch7.
Taylor, C.J., Pedregal, D.J., Young, P.C., Tych, W., 2007. Environmental time series analysis and forecasting with the Captain toolbox. Environ. Modell. Software 22, 797–814, http://dx.doi.org/10.1016/j.envsoft.2006.03.002.
Torrence, C., Compo, G.P., 1998. A practical guide to wavelet analysis. Bull. Am. Meteorol. Soc. 79, 61–78.
Torrence, C., Webster, P., 1999. Interdecadal changes in the ESNO monsoon system. J. Climate 12, 2679–2690.
Tran, N., Labroue, S., Philipps, S., Bronner, E., Picot, N., 2010. Overview and update of the sea state bias corrections for the Jason-2, Jason-1 and TOPEX Missions. Mar. Geod. 33, 348–362.
Trenberth, K.E., 1997. The definition of El Niño. Bull. Am. Meteorol. Soc. 78, 2771–2777.
Tych, W., Pedregal, D.J., Young, P.C., Davies, J., 2002. An unobserved component model for multi-rate forecasting of telephone call demand: the design of a forecasting support system. Int. J. Forecasting 18 (4) 673–695.
Wahr, J.M., 1985. Deformation induced by polar motion. J. Geophys. Res. 90 (B11) 9363–9368.
Xue, Y., Smith, T.M., Reynolds, R.W., 2003. Interdecadal changes of 30-yr SST normals during 1871–2000. J. Climate 16, 1601–1612.
Young, P.C., Pedregal, D.J., Tych, W., 1999. Dynamic harmonic regression. J. Forecasting 18, 369–394.
Young, P.C., Taylor, C.J., Tych, W., Pedregal, D.J., 2007. The Captain Toolbox /sb:title>Centre for Research on Environmental Systems and Statistics, Lancaster University, UK Internet: www.es.lancs.ac.uk/cres/captain.

Further reading

Captain toolbox: http://www.es.lancs.ac.uk/cres/captain. Accessed 13 March 2012.
CU Sea Level Research Group: http://sealevel.colorado.edu. Accessed 14 February 2013.
NCDC ERSST: http://www.ncdc.noaa.gov/ersst. Accessed 14 February 2013.